Validation of MARS-LMR Code for Heat Transfer Models in the DHRS of the PGSFR

Chiwoong CHOI*, Taekeong Jeong, JongGan Hong, Sujin Yeom, Jong-Man Kim, Ji-Yeong Jeong, YongBum Lee and Kwiseok Ha
Korea Atomic Energy Research Institute (KAERI)
111, Daedeok-Daero 989Beon-Gil, Yuseong-Gu, Daejeon, Korea
cwchoi@kaeri.re.kr

ABSTRACT

Korean Atomic Energy Research Institute (KAERI) has developed prototype of Gen-IV sodium-cooled fast reactor (PGSFR), which has a decay heat removal system (DHRS). The DHRS has two types of loops: active and passive types and two heat exchangers are connected on each loop. The one is a sodium-sodium heat exchanger (DHX) and the other is an air-sodium heat exchanger (AHX or FHX). The flows in the active and passive loop are driven by EM-pump and natural circulation, respectively. The air-sodium heat exchanger (AHX) in the passive loop is a helical type. However, the heat exchanger (FHX) in the active loop is a finned serpentine type. KAERI developed a sodium experimental facility, which is called as STELLA, to generate the data to validate the design and safety analysis codes. Recently, the STELLA conducted separation effect tests (SET) for the DHX and AHX. In this study, using these experimental data, the validation of the safety analysis code for the PGSFR, MARS-LMR code is achieved. A different number of nodes are selected to find optimal number of node for the analysis. The results indicate the optimal number of nodes for the DHX is approximately 20 with less 1% RMS error. The MARS-LMR over-estimates the heat transfer rate in the AHX. However, when the correction factor for the deterioration in the entrance region is applied, the estimation becomes better. In the near future, another component including a steam generator will be validated. In addition, a natural circulation test for the DHRS is designing in the STELLA-2 test facility, which will be used to validate MARS-LMR for integration effect test (IET).

KEYWORDS
MARS-LMR, Decay Heat Removal System, DHX, AHX, and FHX

1. INTRODUCTION

Korea Atomic Energy Research Institute (KAERI) has developed a prototype generation-IV sodium-cooled fast reactor (PGSFR) [1]. Figure 1 shows schematics of the PGSFR, which has decay heat removal system (DHRS). The DHRS has four sodium-sodium heat exchangers in a cold pool and four air-sodium heat exchangers in the outside of reactor. And the DHRS consists of two kinds of heat transfer loops: active and passive, named as active DHRS (ADHRS) and passive DHRS (PDHRS), respectively. Sodium-air heat exchangers in the PDHRS and ADHRS are sodium-to-Air Heat eXchanger (AHX) and forced air-sodium heat exchanger (FHX), respectively. The AHX is a helical type bundle heat exchanger and the FHX is a finned serpentine type bundle heat exchanger. Both heat exchangers are cross flow heat

* Corresponding Author

exchanger. A tube and shell sides are sodium and air, respectively. And sodium-sodium heat exchangers in the cold pool, which are named as a decay heat exchanger (DHX) are shell and tube heat exchanger with straight tubes. The DHRS has a role to remove decay heat during accidents. The DHRS is not fully working during a normal operation. Therefore, the damper in the entrance region of the air-sodium heat exchangers is controlled with fail-open logic. In other words, the DHRS can be activated with opening of the damper when the accident occurs. A MARS-LMR code has used as the safety analysis code for the PGSFR. The MARS-LMR has supplemented with pressure drop and heat transfer models related to sodium. KAERI also developed the sodium related experimental facilities called as STELLA-1 to provide validation data for design and safety analysis codes. It has loops for individual heat exchangers, such as AHX and DHX, etc. In this study, the validation tests of the heat transfer models in the MARS-LMR are conducted. Especially, we focused on the heat transfer models in the only the DHX and AHX using recently obtained experimental data from STELLA-1.

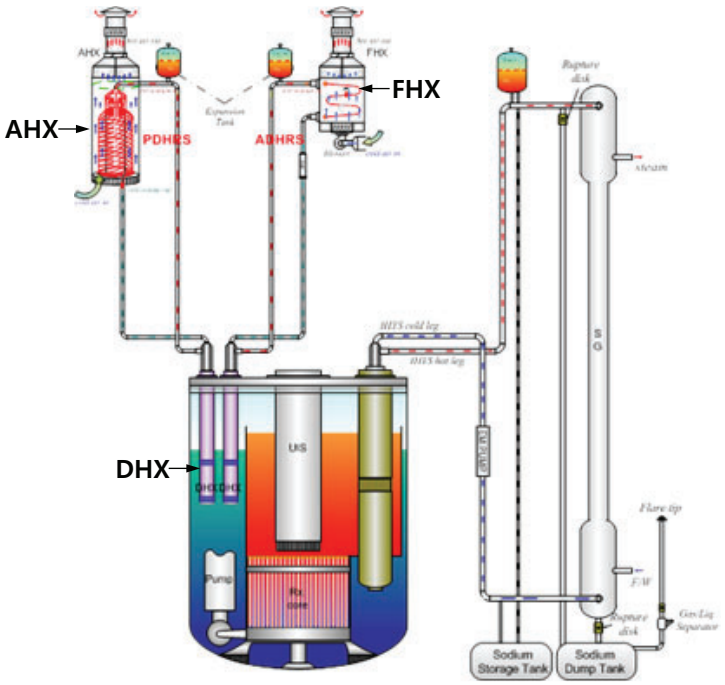

Figure1. Schematic of PGSFR including DHRS

2. Heat Transfer Models in DHRS

The tube and shell side heat transfers models for the DHX are supplemented in MARS-LMR, which is defined as follows [2, 3]:

- Tube: Aoki's correlation

$$Nu_T = 6.0 + 0.025\left[0.014\,\mathrm{Re}^{1.45}\,\mathrm{Pr}^{1.2}\left(1-\frac{e^{-71.8}}{\mathrm{Re}^{0.45}\,\mathrm{Pr}^{0.2}}\right)\right] \quad (1)$$

- Shell: Graber-Rieger's correlation

$$Nu_{DHX-S} = 0.25 + 6.2\left(\frac{P}{D}\right) + \left[0.032\left(\frac{P}{D}\right) - 0.007\right] Pe^{0.8-0.024\frac{P}{D}} \quad (2)$$

The tube-side heat transfer for the AHX is same to the DHX. And Zukauskas' correlation is implemented in MARS-LMR for the shell-side heat transfer model in AHX. The tube rows of a bank can be either in-lined or staggered in the direction of the fluid flow. The configuration is characterized by the tube diameter, D and by the transverse pitch, S_T and longitudinal pitch S_L measured between tube centers as shown in Figure 2. Flow around the tubes in first row of a tube bank is similar to that for a single cylinder in cross flow. Correspondingly, the heat transfer coefficient for a tube in the first row is approximately equal to that for a single tube in cross flow. For downstream rows, flow conditions depend strongly on the tube bank arrangement. In-lined tubes beyond the first row reside in the wakes of upstream tubes, and for moderate values of S_L convection coefficients associated with downstream rows are enhanced by mixing, or tabulation of the flow. Typically, the convection coefficient of a row increases with increasing row number until approximately the fifth row, after with there is little change in flow conditions and hence in the convection coefficient. For large S_L, the influence of upstream rows decrease, and heat transfer in the downstream rows is not enhanced. For this reason, operation of in-lined tube bank with $S_T/S_L < 0.7$ is undesirable. For the staggered tube array, the path of main flow is more tortuous, and mixing of the cross-flowing fluid is increased relative to the in-lined tube arrangement. In general, heat transfer enhancement is favored by the more tortuous flow of a staggered arrangement, particularly for small Reynolds numbers (Re < 100).

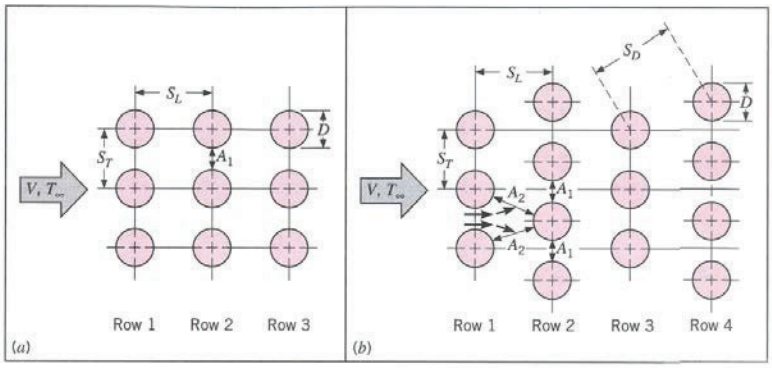

Figure 2. Tube arrangement in a bank: (a) in-lined, (b) Staggered [4]

Zukauskas proposed wide ranged various correlations for bundle flows with following correlation [5].

$$Nu_{AHX-S} = C_1\left(\frac{\mathrm{Pr}_f}{\mathrm{Pr}_w}\right)^{0.25} \mathrm{Re}_{D,\max}^{m}\, \mathrm{Pr}_f^{0.36} \quad (3)$$

where, C_1 is an empirical coefficient, Pr_f is Prandtl number with bulk temperature, Pr_w is Prandtl number with wall temperature, and m is an exponent of Reynolds number, which is defined with maximum velocity and single tube outer diameter.

$$\mathrm{Re}_{D,\max} = \frac{\rho V_{\max} D}{\mu} \quad (4)$$

C_1 and m is proposed with Reynolds number for the arrangement type as shown in Table I.

Table I. Constants of Zukauskas' bundle correlation (Eq.3)

Configuration	$Re_{D,max}$	C_1	m
Aligned	1.6 – 100	0.9	0.4
Aligned	100 - 1000	0.52	0.5
Aligned (S_T/S_L>0.7)	1000 - 2×10^5	0.27	0.63
Aligned	2×10^5 - 2×10^6	0.033	0.8
Staggered	1.6 - 40	1.04	0.4
Staggered	40 - 1000	0.71	0.5
Staggered (S_T/S_L<2)	1000 - 2×10^5	$0.35(S_T/S_L)^{0.2}$	0.6
Staggered (S_T/S_L>2)	1000 - 2×10^5	0.4	0.6
Staggered	2×10^5 - 2×10^6	0.031	0.8

3. Validation Data from STELLA Facility

3.1. DHX

The DHX is a shell-and-tube type heat exchanger, which transports the heat from the hot pool to the AHX. As shown in Figure 3, the sodium flow in the shell-side comes from top to bottom. The sodium flow in the tube-side comes thru the down-comer in the center region and distributed to each straight tubes in the annular region. Therefore, the DHX is a counter-current flow type heat exchanger. The inlet and outlet regions in the actual DHX are modified to two tubes in each region in the STELLA-1 assuming the disturbance of flow distribution in the inlet region is negligible as shown in Figure 3. The DHX in the STELLA-1 facility is designed to conserve the major heat transfer phenomena in the actual PGSFR. So, any scaling law is not applied to the DHX in the STELLA-1. The various inlet temperatures and flow rates are selected based on the operational range of the DHX in the PGSFR. Figure 4 shows Reynolds and Prandtl numbers for the operational condition of the PGSFR and experimental conditions of the STELLA-1. The test cases in the DHX of STELLA-1 are covered in the range of the PGSFR. Considering the accident conditions, the wider range is selected. Major design parameters of the DHXs in the PGSFR and the STELLA-1 are summarized in Table II.

The Figure 5 shows the nodalizations of MARS-LMR for the DHX of STELLA-1. The number of nodes and junctions in shell and tube region are 45 and 43, respectively. The shell-side boundary volumes for inlet and outlet are modeled with volume no. 100 and 120, respectively. And the tube-side boundary volumes for inlet and outlet are modeled with volume no. 200 and 290, respectively. In addition, the heat structure between the shell and tube is modeled to consider heat transfer between shell and tube with implemented heat transfer correlations, as described in Chapter 2.

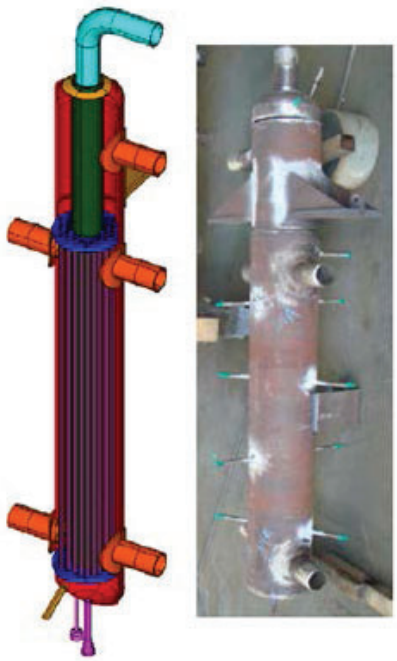

Figure 3. Schematics of the DHXs in the PGSFR and STELLA-1

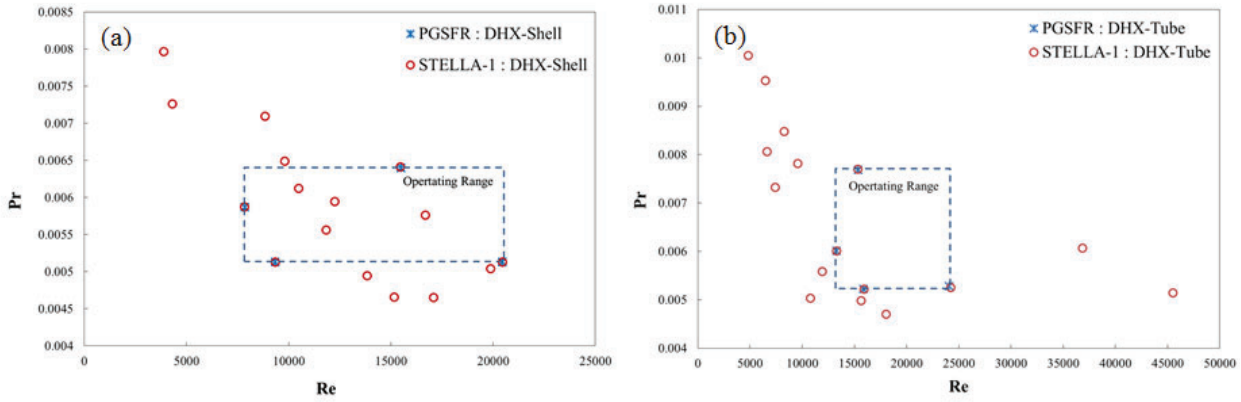

Figure 4. Reynolds and Prandtl numbers of the DHXs of PGSFR and STELLA-1: (a) shell-side, (b) tube-side

Table II. Conditions of the DHXs in the PGSFR and the STELLA-1

DHX		PGSFR				STELLA-1	
		Normal Condition		Accident Condition			
		Inlet	Outlet	Inlet	Outlet	Inlet	Outlet
Shell	Temperature [℃]	390.0	265.8	390.0	307.2	215.0 ~ 475.0	183.7 ~ 316.9
	Mass Flow [kg/s]	2.84		6.22		2.00~6.22	
	I.D [m]	0.289		0.289		0.2889	
	O.D of the annular [m]	0.1413		0.1413		0.1413	
Tube	Temperature [℃]	195.6	370.2	295.1	377.4	120.8 ~ 295.1	211.9 ~ 464.0
	Mass Flow [kg/s]	2.85		4.38		1.84~8.00	
	O.D [m]	0.0217		0.0217		0.0217	
	Thickness [m]	0.00165		0.00165		0.00165	
	I.D [m]	0.0184		0.0184		0.0184	
	The number of tubes [EA]	42		42		42	

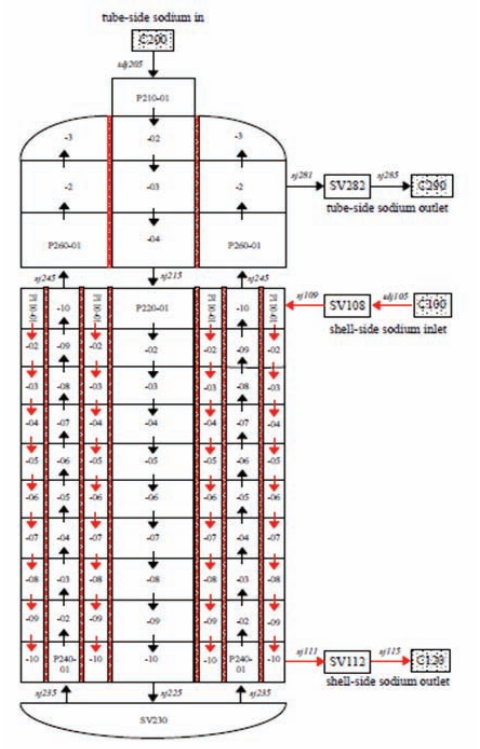

Figure 5. Nodalization of MARS-LMR for the DHX in the STELLA-1

3.2. AHX

The helical type sodium-to-air heat exchanger (AHX) has a role to transport the heat, which is gain from connecting pipe with the DHX submerged into the hot pool, to the ultimate heat sink, ambient air. The helical structure has reliability for thermal expansion and contraction and efficiency for heat transfer due to larger heat transfer area. In addition, the heat transfer enhancement can be achieved with cross-flow thru tube buddle comparing to a parallel flow thru a straight tube. And the AHX is a shell-and-tube type heat exchanger with counter-current flow. As shown in Figure 6, helical tubes are positioned in annular shaped shell region. The sodium flow is distributed to tubes thru the upper sodium chamber. Then, the sodium in each helical tube flows downward to lower chamber. The air flow entered from the lower entrance, then pass thru the annulus shell region, finally, go out to the ambient. The major heat transfer occurs in the counter-current flow region. The AHX in the STELLA-1 facility is designed to conserve the major heat transfer phenomena in the actual PGSFR. Based on a scaling law, the tube diameter, thickness, and alignment are identically maintained to those in the PGSFR. The power and flow are reduced to 50% in order to conserve the temperature difference between inlet and outlet temperatures. Figure 7 shows Reynolds and Prandtl numbers for the operational condition of the PGSFR and experimental conditions of the STELLA-1. The test cases in the AHX of STELLA-1 are covered in the range of the PGSFR. Considering the accident conditions, the wider range is selected.

The Figure 8 shows nodalizations in the MARS-LMR for the AHX in the STELLA-1. The effective heat transfer region is modeled with 40 volumes and 38 junctions as reference. Volume no. 205 and 260 indicates the inlet and outlet in the shell side, respectively. And Volume no. 105 and 140 indicates the inlet and outlet in the tube side, respectively. As shown in Table III, all inlet flows and temperatures of 29 experimental cases are applied in the validation calculation. And the heat structure with heat transfer models described in chapter 2 is modeled.

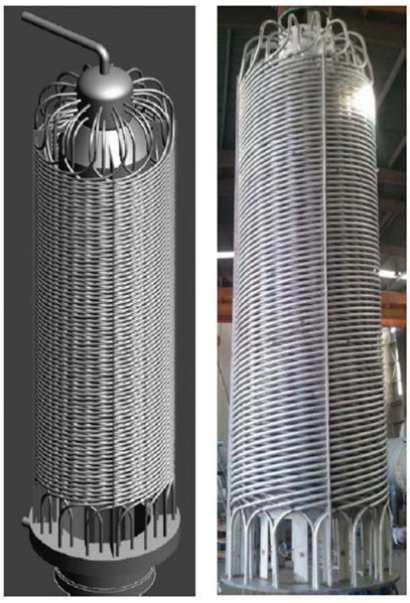

Figure 6. Schematics of AHXs in the PGSFR and STELLA-1

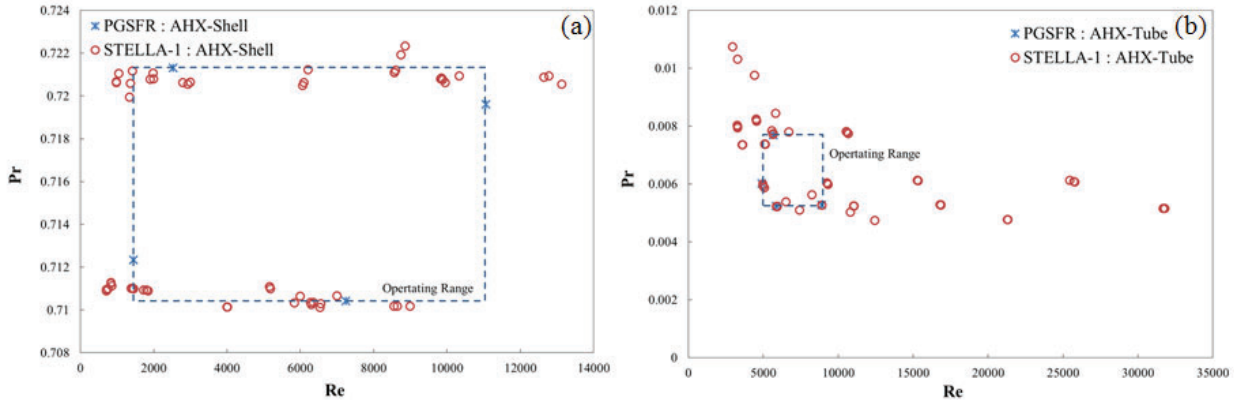

Figure 7. Reynolds and Prandtl numbers of the AHXs of PGSFR and STELLA-1: (a) shell-side, (b) tube-side

Table III. Conditions of the AHXs in the PGSFR and the STELLA-1

AHX		PGSFR				STELLA-1	
		Normal Condition		Accident Condition			
		Inlet	Outlet	Inlet	Outlet	Inlet	Outlet
Shell	Temperature [℃]	40.0	289.7	20.0	362.8	8.2 ~ 36.0	185.2 ~ 330.5
	Mass Flow [kg/s]	0.89		4.09		0.35~4.71	
	Longitudinal Pitch, SL [m]	0.05814		0.05814		0.05814	
	Transverse Pitch, ST [m]	0.085		0.085		0.085	
	I.D [m]	1.53		1.53		1.530	
	O.D of the annular [m]	0.98		0.98		0.981	
Tube	Temperature [℃]	370.2	195.6	377.4	295.1	209.1 ~ 455.5	105.7 ~ 307.0
	Mass Flow [kg/s]	2.85		4.38		1.39~8.02	
	O.D [m]	0.034		0.034		0.034	
	Thickness [m]	0.00165		0.00165		0.002	
	I.D [m]	0.0307		0.0307		0.031	
	The number of tubes [EA]	68		68		36.000	

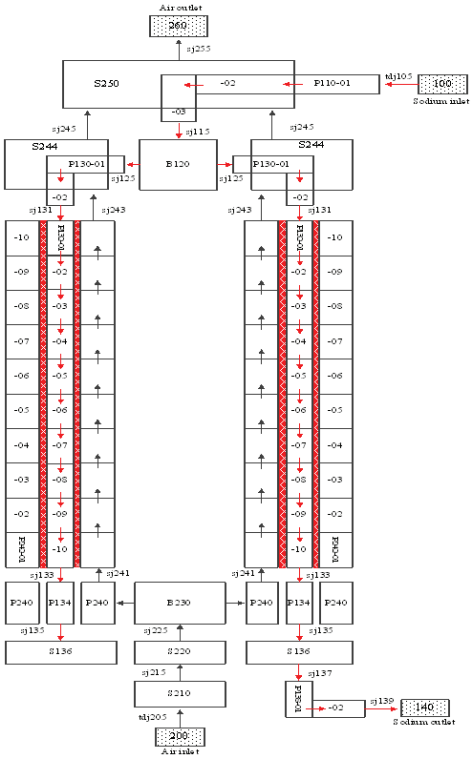

Figure 8. Nodalization in MARS-LMR of the AHXs in the STELLA-1

4. Validation Result of MARS-LMR

4.1. Validation Result for DHX

The comparison between MARS-LMR analysis and STELLA-1 experiment is performed with temperature difference of inlet and outlet and log-mean temperature difference (LMTD). Figure 9 and 10 show comparison results of temperature differences of inlet and outlet and LMTD, respectively. The validation results indicate good agreements for the DHX with deviation of less than 1%. In addition, the node size effect in the heat structure region is studied with the number of nodes of 10 – 60. As shown in Figure 11, the results with the number of nodes of 30 show better prediction.

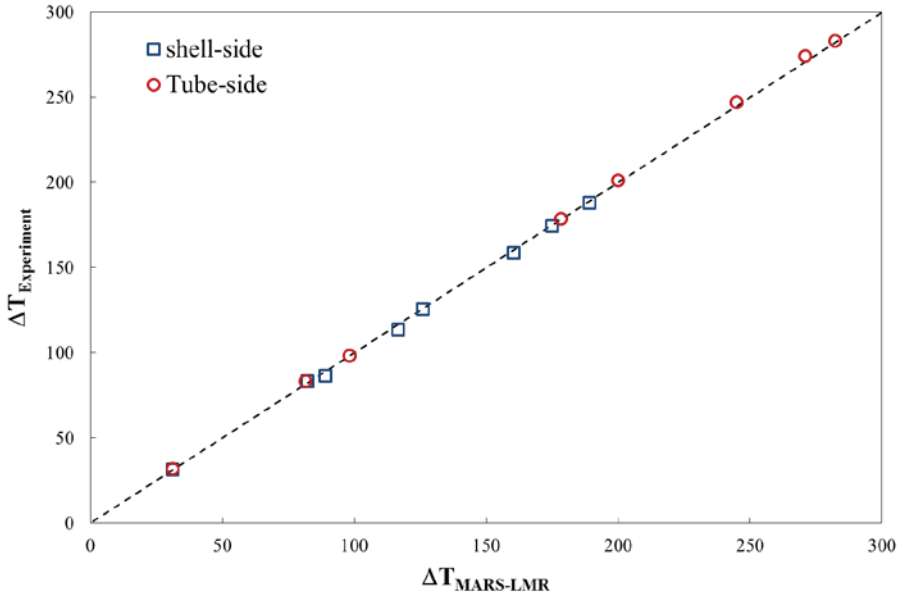

Figure 9. Comparison of temperature changes in tube/shell side of the DHX

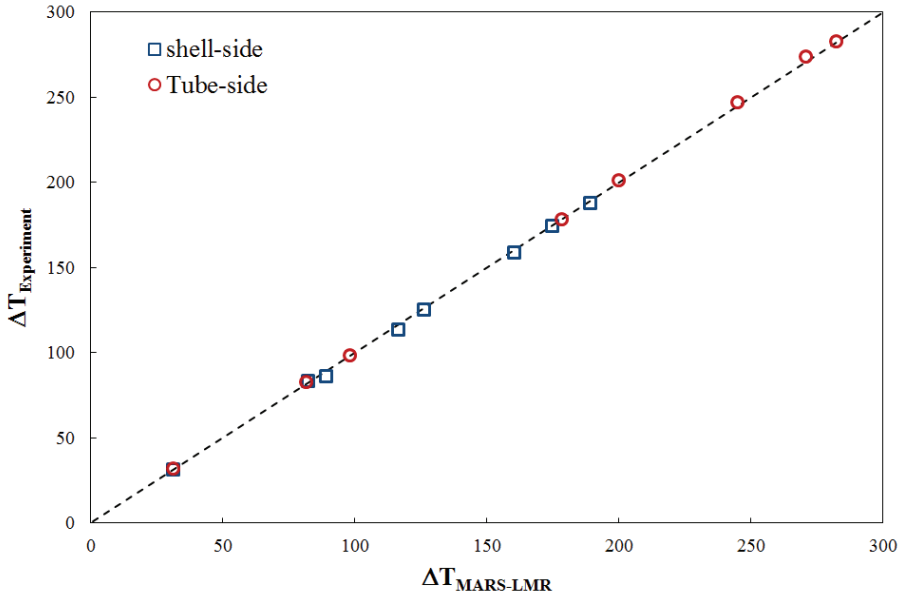

Figure 10. Comparison of LMTD temperatures of the DHX

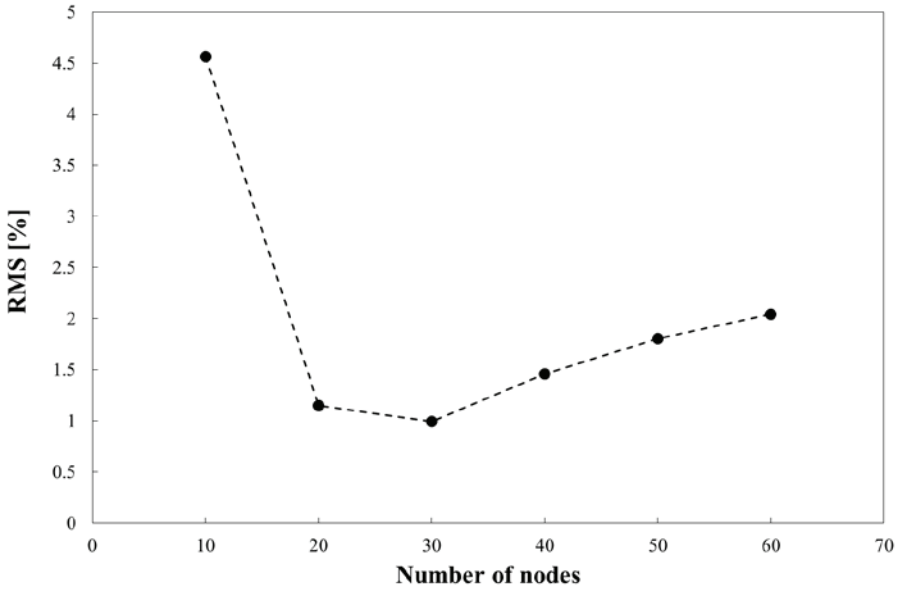

Figure 11. RMS values for the different number of nodes for the DHX

4.2. Validation Result for AHX

The comparison between analysis of MARS-LMR and experiment for the AHX are conducted with same temperature differences to those in the DHX. Figure 12 and 13 show comparison results of the AHX between the MARS-LMR and STELLA-1 experiment with temperature differences of inlet and outlet and LMTD, respectively. The largest deviation of LMTD in validation calculation is 18.4 %. Figure 14 shows the deviations for air and sodium flow rate conditions. The largest deviations are shown in the low air and sodium flow rate conditions, which is less than the normal operation conditions as shown in Table III. Except these data, the rest of results are included in 1-2 %, which is marked as refined data in Figure 13. Considering the measurement uncertainties for the AHX in the STELLA-1, the low flow rate condition can have a larger influence. Especially, the air flow rate measurement is the relatively larger uncertainty parameter. Recently, STELLA-1 experiment team has a plan to improve the accuracy in the experimental data for specific conditions.

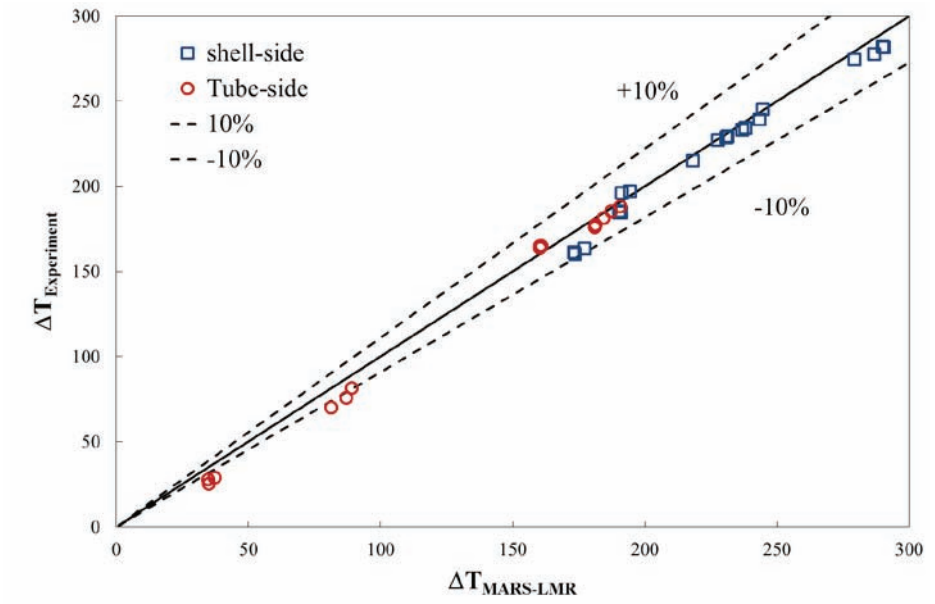

Figure 12. Comparison of temperature changes in tube/shell side of the DHX

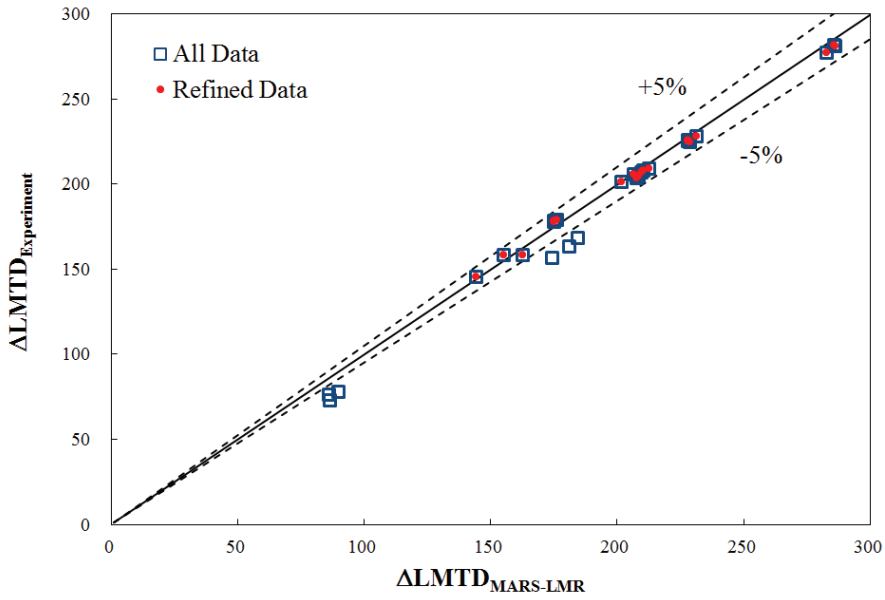

Figure 13. Comparison of LMTD temperatures of the DHX

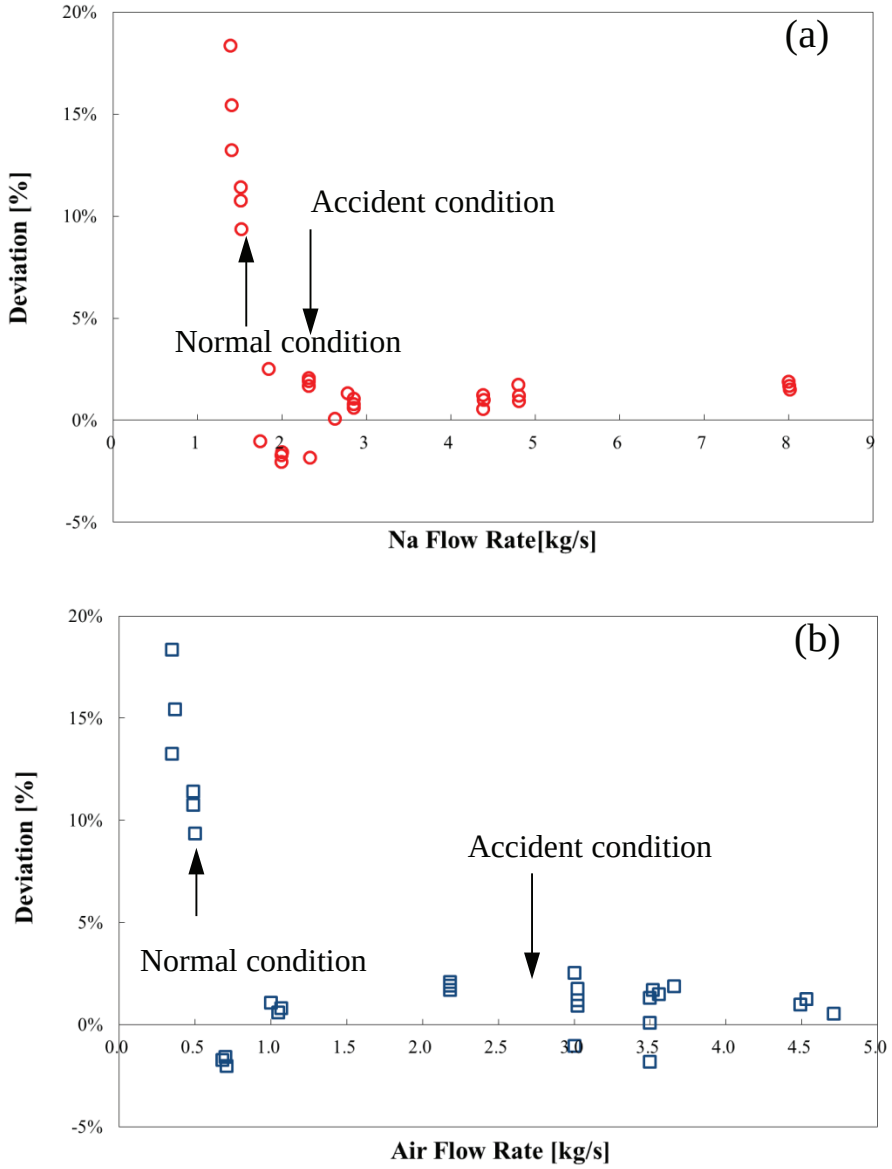

Figure 14. Deviations between MARS-LMR and experiment for flow rates in AHX : (a) sodium flow rate [kg/s], (b) air flow rate [kg/s]

5. CONCLUSIONS

The heat transfer models for the heat exchangers in DHRS are implemented in MARS-LMR, has used for the safety analysis of the PGSFR. In this study, MARS-LMR is validated with the experimental data obtained from STELLA-1 facility. Especially, the heat exchangers in the DHRS: DHX and AHX are focused on this study. Aoki's correlation is applied in tube-side in both the DHX and the AHX. Graber-Rieger's and Zukauskas' correlations are applied in shell-sides in the DHX and the AHX, respectively. From the validation results, the heat transfer models for the DHX in MARS-LMR is well agreed with experimental results. Especially, when 30 nodes is applied in heat transfer region, the RMS values shows minimum, which is about 1% of RMS. The validation results for the heat transfer models of the AHX in MARS-LMR shows slightly larger deviation from experimental results than that in the DHX. The RMS

value of the AHX is 6.3%. However, the larger deviation is observed in lower flow rates, which are same or lower to the normal operation conditions. Except the lower flow rate cases, the RMS value of the AHX is 1.5%, which shows much better prediction. Considering a larger uncertainty of low flow rate, especially air flow rate, the STELLA-1 experiments for the AHX will be re-evaluated.

NOMENCLATURE

Nu_T	Nusselt number for tube-side
Nu_{DHX-S}	Nusselt number for shell-side in the DHX
Nu_{AHX-S}	Nusselt number for shell-side in the AHX
Re_f	Fluid Reynolds number
$Re_{D,max}$	Reynolds number for maximum velocity
Pr_f	Fluid Prandtl number
Pr_w	Wall Prandtl number
P	tube pitch
D	tube diameter
V_{max}	maximum velocity
S_T	Transverse pitch
S_L	Longitudinal pitch

ACKNOWLEDGMENTS

This work was supported by the Nuclear Research & Development Program of the National Research Foundation (NRF) grant funded by the Korean government MSIP (Ministry Science, ICT and Future Planning).

REFERENCES

1. Yeong-il Kim, Yong Bum Lee, Chan Bock Lee, Jinwook Chang, and Chiwoong Choi, Advanced Design Concept of Sodium-Cooled Fast Reactor and Related R&D in Korea, *Science and Technology of Nuclear Installations*, Vol. 2013 (2013).
2. S. Aoki, Current Liquid-metal Heat Transfer Research in Japan, *Prog. Heat Mass Transfer*, Vol.7, (1973).
3. H. Graber and M. Rieger, Experimentelle Untersuchung des Warmeubergangs an Flussigmetall (NaK) in parallel durchstromten Rohrbundeln bei konstanter und exponentieller Warmeflussdichteverteilung, *Atomkernenergie*, Vol. 19, pp. 23-30 (1972)
4. F.R. Incropera and D. P. Dewitt, *Fundamentals of Heat and Mass Transfer*, John Wiley and Sons, (2011).
5. A. Zukauskas and J. Karni, *High-performance Single-phase Heat Exchangers*, Hemisphere Publishing Corporation, (1989).